

Article

Behavior of Concrete-Filled Steel Tube Columns with Multiple Chambers and Round-Ended Cross-Sections under Axial Loading

Jing Liu ^{1,2}, Tao Zhang ³, Zhicheng Pan ^{4,5,*} and Fanjun Ma ⁴

¹ Key Laboratory of Green Building and Intelligent Construction in Higher Educational Institutions of Hunan Province, Hunan City University, Yiyang 413000, China; liujing@hncu.edu.cn

² A Dual Innovation Platform Combining Production, Education and Research with Science and Technology of the Construction Industry of Hunan Province, Hunan City University, Yiyang 413000, China

³ School of Civil Architecture, Zhengzhou University of Aeronautics, Zhengzhou 450000, China; zhangtao0226@zua.edu.cn

⁴ Sinohydro Engineering Bureau 8 Co., Ltd., Changsha 410004, China; mafanjun@126.com

⁵ Power China Chizhou Changzhi Prefabricated Construction Co., Ltd., Chizhou 247100, China

* Correspondence: panzhichengcsu@163.com

Abstract: Concrete-filled round-ended steel tubes (CFRTs) are a unique type of composite stub columns, which have the advantage of aesthetics and a well-distributed major–minor axis. Thus, the structure has been widely employed as piers and columns in bridges. To improve the mechanical performance of CFRTs with a large length–width ratio and to enhance the restraint effect of steel tubes on concrete, this study investigates the compressive property of multi-chamber, concrete-filled, round-ended steel tubular (M-CFRT) stub columns using a combination of experimental and numerical analyses. A detailed compression test on eight specimens is conducted to examine the compressive property of M-CFRT stub columns. The study focuses on understanding the influence of some key parameters on ultimate bearing capacity, failure stage, damage modes, and ductility. Additionally, the accuracy of the finite element modeling method in simulating the ultimate bearing capacity of the structure is verified. Finally, the calculating formula for the ultimate bearing capacity of M-CFRT stub columns is proposed on the basis of the experimental and numerical findings. Results of the formula calculation are consistent with the experimental data. These research findings serve as a valuable reference for designing similar structures in engineering practice.

Keywords: concrete-filled round-ended steel tubular stub column; multi-chamber steel tube; ultimate bearing capacity



Citation: Liu, J.; Zhang, T.; Pan, Z.; Ma, F. Behavior of Concrete-Filled Steel Tube Columns with Multiple Chambers and Round-Ended Cross-Sections under Axial Loading. *Buildings* **2024**, *14*, 846. <https://doi.org/10.3390/buildings14030846>

Academic Editor: Oldrich Sucharda

Received: 24 January 2024

Revised: 27 February 2024

Accepted: 14 March 2024

Published: 21 March 2024



Copyright: © 2024 by the authors. Licensee MDPI, Basel, Switzerland. This article is an open access article distributed under the terms and conditions of the Creative Commons Attribution (CC BY) license (<https://creativecommons.org/licenses/by/4.0/>).

1. Introduction

Round-ended reinforced concrete columns have a suitable major–minor axis distribution, a low flow resistance coefficient, and an attractive appearance; thus, this structure has been employed extensively as piers and columns in bridge engineering over the past decades [1–3]. However, building it is a highly difficult procedure that requires substantial formwork, particularly at the beam–column joints. Furthermore, as heavy haul railroads and tall bridges grow in popularity, the need for piers to have a certain bearing capacity, ductility, and anti-seismic property increases. Concrete-filled steel tubes are a good choice, due to their excellent mechanical properties and convenient construction characteristics [4–6].

A novel type of composite stub column, known as concrete-filled, round-ended steel tube (CFRT) stub columns, was proposed against this background. Given their rounded edges, CFRT members have high architectural aesthetic and may successfully lessen the influence of fluid load on the pier. In addition, CFRT stub columns can offer the benefit of not requiring a reinforced cage or formwork. In this construction method, permanent and integral formworks can be achieved by using external steel tubes, which can function

as permanent and integral formworks, resulting in decreased labor costs, materials, and construction time. As a result of these advantages, CFRT stub columns have recently garnered increasing interest from domestic and foreign researchers and engineers and have been used in bridge construction, as demonstrated by the Weihe Bridge in Baoji City, China, the Houhu Cable-stayed Bridge in Wuhan, China, and the Platform of the Xinglin Gulf in Xiamen City, China (illustrated in Figure 1) [7,8].

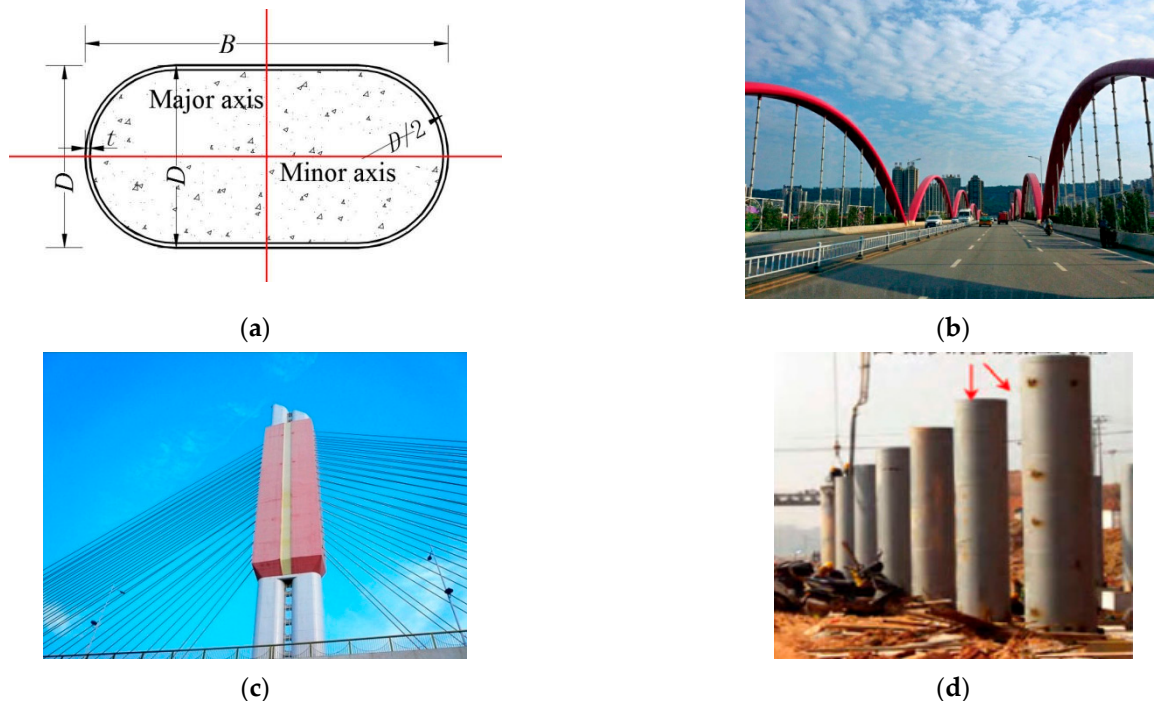


Figure 1. Illustrations and typical applications of CFRT members. (a) Cross-section of CFRTs. (b) Weihe bridge in Baoji City. (c) Cable-stayed bridge in Wuhan city. (d) Xinglin Gulf in Xiamen City.

In actual engineering, the axial compression performance is a key property for structures. To date, numerous experimental and finite element analysis (FEA) research have been conducted on the property of CFT stub columns or other structures under axial compression, and the research provided ideas for this study [9–17].

However, to the author's best knowledge, not many studies have been published on CFRT stub columns. Xie et al. [7,8] investigated the behavior of paired RECFST columns during the time of the construction of the Houhu Cable-stayed Bridge. Zhou et al. [18] conducted experimental studies on the compressive behavior of concrete-filled single-skin and double-skin steel tubular stub columns, and they also explored the effects of concrete strength and geometric dimension. Ding et al. [3] studied the behavior of CFRT stub columns under axial compression through experimental and numerical investigations and also suggested a simplified streamline for determining the ultimate carrying capacity. Han et al. [19] tested round-ended concrete, stainless steel, carbon steel, and multi-skin stub columns. They discovered that the composite stub columns exhibited strong bearing capacity and good ductility. In addition, Wang et al. [20] and Ding et al. [21] conducted a numerical investigation on the compressive properties of CFRT stub columns and proposed a novel method, which involves the welding of bidirectional stirrups to the inner surface of the round-ended steel tube, resulting in track-shaped, rebar-stiffened, concrete-filled, round-ended steel tubular stub columns. The analysis results demonstrated that the novel approach can successfully avert local buckling and enhance the overall ultimate carrying capacity.

Previous studies have found that welding work between the steel tubes and stirrups is a challenging task in practical engineering [20]. Additionally, as the aspect ratio (B/D) increases, the function of restraint of the steel tube on the core concrete decreases, and when the section aspect ratio of a round-ended CFST column is greater than 5.0, the constraints to the core concrete by a single-cavity steel tube becomes negligible, leading to an increased severity of the local buckling of the steel tube [3,21]. This issue makes it difficult to use the columns in engineering applications. To address these issues, this study proposes a new method to enhance the compressive property of composite stub columns, hereafter called multi-chamber, concrete-filled, round-ended steel tubular (M-CFRT) stub columns, as shown in Figure 2. However, the compressive behavior of these columns is currently unknown, and the effect of vertical diaphragms must also be investigated.

Through these research activities, the study aims to fill the research gaps and provide valuable insights into the design and utilization of M-CFRT stub columns in practical engineering. Specifically, on the basis of the experimental and numerical data results from our research group [3,21], the major objectives of this study are as follows: (1) explore the mechanical performances of the composite columns by conducting axial compression tests on eight specimens with different preformed chambers, (2) investigate the axial loading behavior by developing FE models based on the experimental results, and (3) derive a simplified formula for predicting the ultimate carrying capacity by applying ratio simplification in accordance with the superposition principle and on the basis of the tested and numerical consequences [3,17].

2. Experimental Investigation

2.1. Test Specimen

This study involved the design and testing of a total of eight specimens to examine the axial compressive properties of the M-CFRT stub columns. The effects of chamber construction and aspect ratio (B/D) were considered. Figure 2 shows the cross-section dimensions of the M-CFRT stub columns, and Table 1 provides the detailed information for each specimen. In the table, B represents the out-to-out dimension in the minor axis direction, while D represents the out-to-out dimension in the major axis direction and the diameter of the two semicircles of the cross-section. t denotes the parameter indicating the thickness of the steel tube and the vertical diaphragm, whereas L signifies the height of the specimen in millimeters. f_y stands for the yield strength of the steel, and f_{cu} represents the cube strength of the concrete. Expressed as the quotient of the steel tube area divided by the total cross-sectional area, the steel ratio is denoted as p_s . The ultimate bearing capacity of the specimens subjected to testing is represented by N_U .

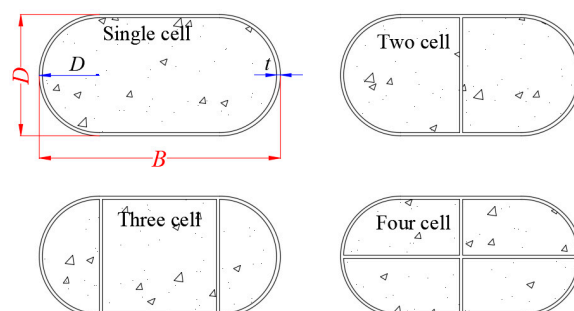


Figure 2. Cross-section of M-CFRT stub columns.

The fabrication of multi-chamber round-ended steel tubes consisted of two steps. Initially, U-shaped cross-sections were formed from the flat steel plates. Subsequently, two U-shaped cross-sections and several vertical diaphragms were joined together using single-bevel butt welds. The choice to use butt welds followed the guidelines specified in the standard GB 50017-2003 [22].

Table 1. Geometric properties and characteristics.

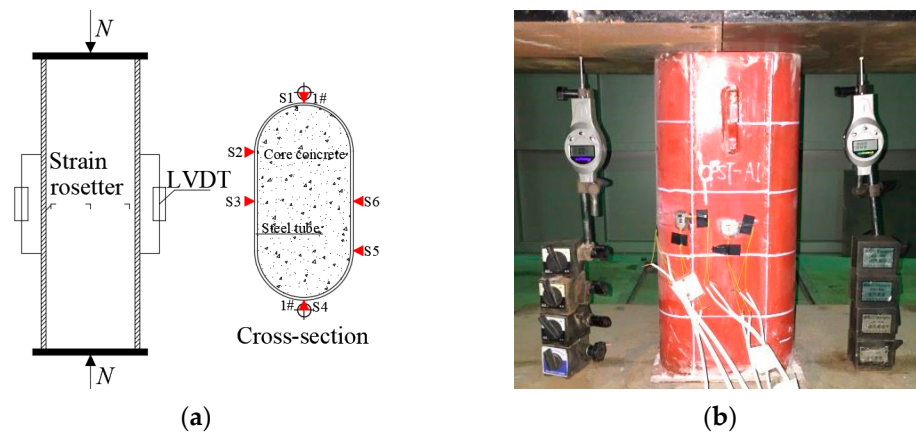
No.	Specimen ID	$B \times D \times t \times H/\text{mm}$	B/D	Chamber	f_s	f_{cu}	ρ_s	$N_{u,e}/\text{kN}$															
1	CFST-A1	$228 \times 114 \times 4 \times 500$	2	1	334	37	10.1	1420															
2	CFST-A2	$228 \times 114 \times 4 \times 500$	2	2	334	37	12.1	1740															
3	CFST-A3	$228 \times 114 \times 4 \times 500$	2	3	334	37	14.0	1800															
4	CFST-A4	$228 \times 114 \times 4 \times 500$	2	4	334	37	16.0	1930															
5	CFST- A5	$342 \times 114 \times 4 \times 500$	3	1	334	37	9.0	1830															
6	CFST- A6	$342 \times 114 \times 4 \times 500$	3	2	334 </tr <tr> <td>7</td> <td>CFST- A7</td> <td>$342 \times 114 \times 4 \times 500$</td> <td>3</td> <td>3</td> <td>334</td> <td>37</td> <td>11.5</td> <td>2510</td> </tr> <tr> <td>8</td> <td>CFST- A8</td> <td>$342 \times 114 \times 4 \times 500$</td> <td>3</td> <td>4</td> <td>334</td> <td>37</td> <td>14.0</td> <td>2715</td> </tr>	7	CFST- A7	$342 \times 114 \times 4 \times 500$	3	3	334	37	11.5	2510	8	CFST- A8	$342 \times 114 \times 4 \times 500$	3	4	334	37	14.0	2715
7	CFST- A7	$342 \times 114 \times 4 \times 500$	3	3	334	37	11.5	2510															
8	CFST- A8	$342 \times 114 \times 4 \times 500$	3	4	334	37	14.0	2715															

2.2. Material Properties

Before the trial, the mechanical properties of the materials, including steel plate and concrete, were determined through material testing using standard methods. Mild steel was the type of steel used in this study, and three tensile coupons were cut to obtain the material properties of the steel tube used in the specimens. Additionally, the cubic compressive strength (f_{cu}) of concrete was obtained by testing concrete cubes. Further details regarding the material properties are summarized in Table 1.

2.3. Experimental Instrumentation

Axial compression experiments were conducted on eight specimens utilizing a universal pressure testing machine with a 500-ton capacity in the National Demonstration Center for Experimental Civil Engineering Education at Hunan City University. For the precise deformation measurement of the specimens, six strain rosettes (S) were affixed to the mid-height of the columns, and two LVDTs were affixed at an identical position, as illustrated in Figure 3. Meanwhile, the DH3818 static strain measurement system was used to obtain axial load vs. strain curves, while electronic transducers and a data acquisition system were used to collect axial load vs. deformation curves.

**Figure 3.** Experimental instrumentation for all specimens. (a) Schematic view. (b) Experimental setup.

All specimens were tested under monotonic static loading, and the compressive load was applied to the top of the specimens through a load control mode. First, the load increased by a step of $1/20$ of the expected ultimate load in the elastic stage. Second, the load was applied to the specimens via displacement control, with an increment of 0.2 mm after reaching approximately 60% of the expected ultimate bearing capacity. Each loading step lasted 3–5 min. When the load was up to the ultimate bearing load, the specimen was loaded slowly and continuously at a step of 0.5 mm, and data were recorded continuously for 5 min. Finally, the tests were stopped when the axial strain reached 0.04, which was the maximum strain of the specimens. The entire loading time for each specimen was approximately 1.5 h, utilizing the experimental configuration adopted from Ding et al. [3].

3. Experimental Results Analysis

3.1. Failure Stages

Figure 4 shows the axial load–strain curves of the specimens, where the compression of composite stub columns exhibited a consistent pattern. Consequently, it was segmented into three distinct stages: the elastic stage, the elastic–plastic stage, and the failure stage.

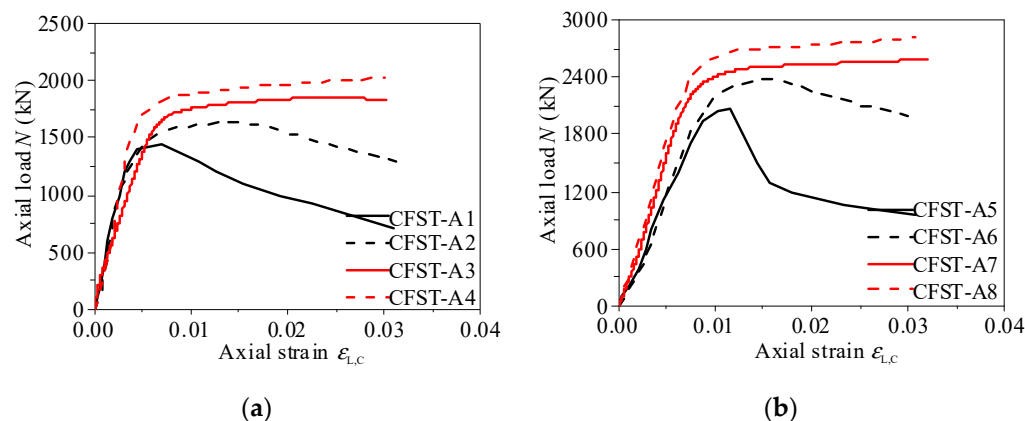


Figure 4. Axial load–strain curves of specimens. (a) CFST-A1~CFST-A4 specimens. (b) CFST-A5~CFST-A8 specimens.

Stage I: During the elastic phase, the elastic modulus of all specimens remained constant. The imposed load increased quickly, whereas the elastic displacement was close to zero.

Stage II: In the elastic–plastic phase, as the applied load approached approximately 60–70% of the peak value, the steel tube initiated yielding. Subsequently, the axial load–strain curves manifested an elastic–plastic behavior.

Stage III: When the peak value was reached, the applied load decreased sharply as the displacement continued to increase. This phenomenon primarily resulted from the core concrete failure, coupled with the steel tube buckling.

3.2. Damage Modes

Figure 5 illustrates the characteristic failure modes observed in all examined specimens. As depicted, the failure modes among CFRT stub columns (such as specimens CFST-A1 and CFST-A5) and M-CFRT stub columns (such as specimens CFST-A2–CFST-A4 and CFST-A6–CFST-A8) were virtually indistinguishable overall. All the specimens showed remarkable axial compression deformation, and the outer steel tube exhibited local buckling.

After the compression test was stopped, the outer steel tube was cut off, and then the condition of the core concrete was observed, as shown in Figure 6. At first, the CFST-A1 specimen had an inclined shear rupture zone and/or even crushes in the core concrete, and the composite stub column could no longer withstand the axial load, as shown in Figure 6a. The analytical results demonstrated that the steel tube with a single cell cannot provide a sufficient confinement effect on the core concrete and therefore cannot effectively prevent the formation of the shear sliding crack in the core concrete. In addition, for the CFST-A2, CFST-A3, and CFST-A4 specimens, the core concrete was crushed only at the area of local buckling, as shown in Figure 6b–d, yet the core concrete remained intact due to the confinement effect of the steel tube. Therefore, the multicell steel tube helps enhance the confinement effect on the core concrete, fundamentally preventing the shear cracks in the core concrete from expanding rapidly and changing the failure mode of the composite stub columns.

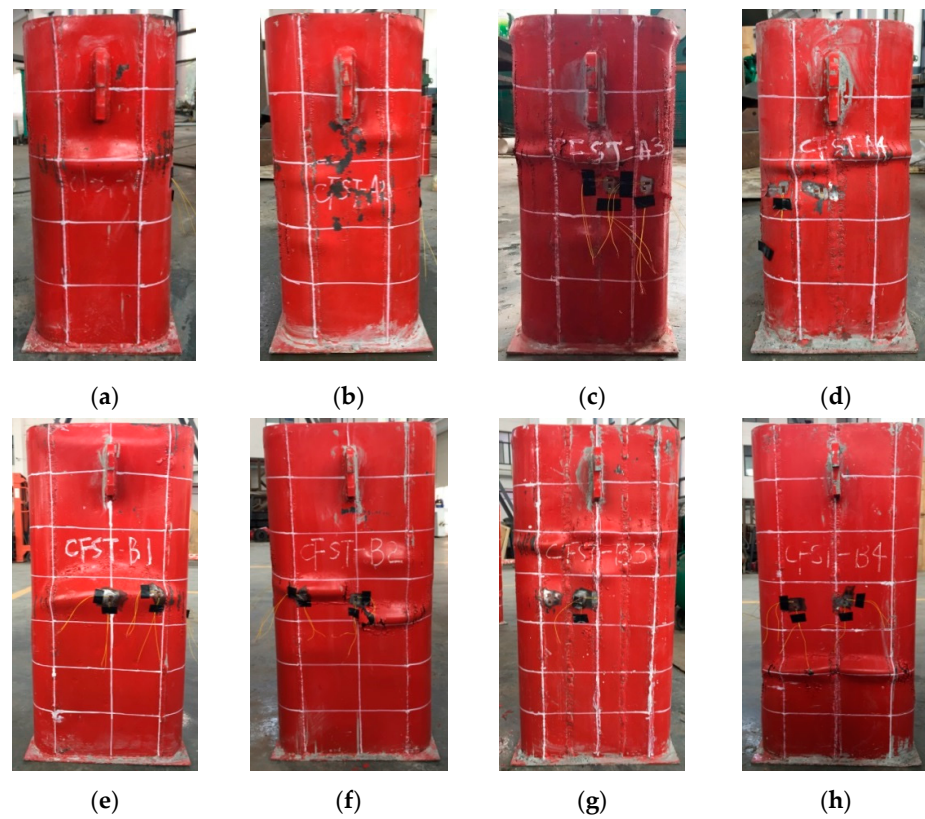


Figure 5. Typical failure modes for tested specimens. (a) CFST-A1. (b) CFST-A2. (c) CFST-A3. (d) CFST-A4. (e) CFST-A5. (f) CFST-A6. (g) CFST-A7. (h) CFST-A8.

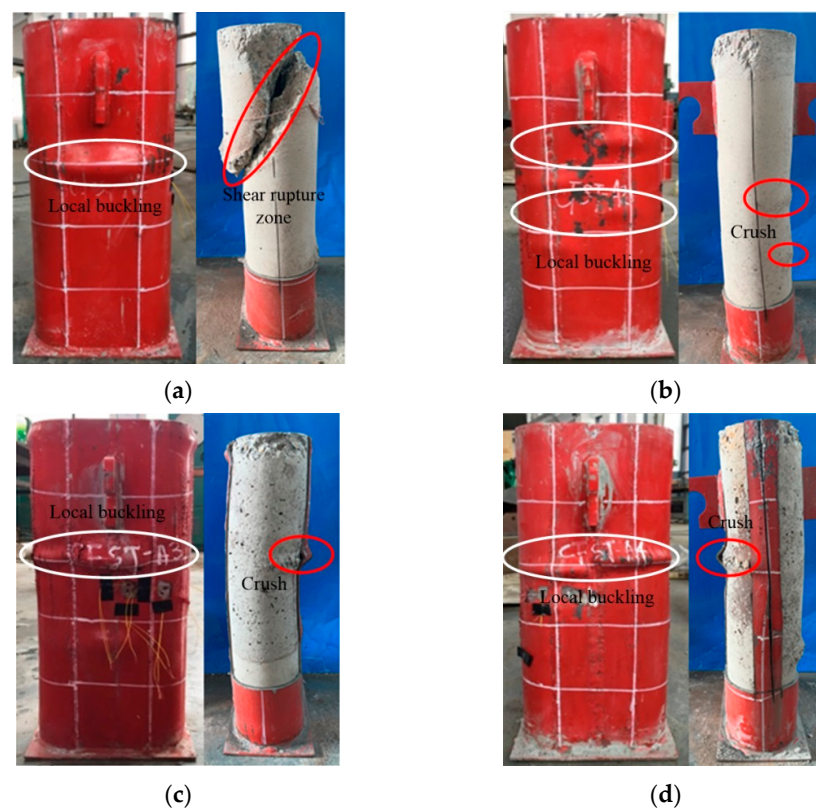


Figure 6. Typical failure modes for core concrete. (a) CFST-A1. (b) CFST-A2. (c) CFST-A3. (d) CFST-A4.

3.3. Ultimate Carrying Capacity

The presence of the multi-chamber steel tube stands out as a distinctive feature in M-CFRT stub columns, considerably setting them apart from conventional CFRT stub columns. Therefore, the multi-chamber steel tube, which affects the compressive behavior of M-CFRT stub columns, is discussed in detail in this section. Figure 7 shows the effects of chamber numbers and aspect ratio on the ultimate carrying capacity.

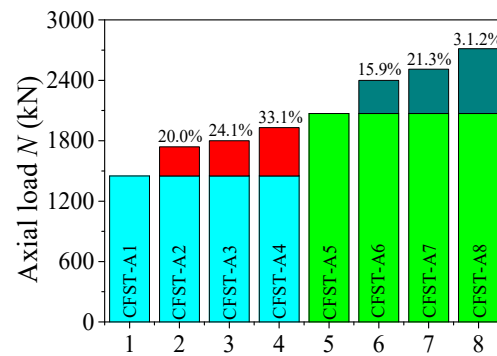


Figure 7. Comparison of ultimate carrying capacity for all specimens.

The number of chambers within the steel tube was considered while maintaining consistency with the aforementioned parameters. Compared with the ultimate carrying capacity of CFST-A1, those of CFST-A2, CFST-A3, and CFST-A4 were improved by 20.0%, 24.1%, and 33.1%, respectively, with the chamber number of the steel tube increasing from 1 to 2, 3, and 4. In addition, compared with the peak capacity of CFST-A5, those of CFST-A6, CFST-A7, and CFST-A8 were improved by 15.9%, 21.3%, and 31.2%, respectively, as the chamber number of the steel tube increased from 1 to 2, 3, and 4. Therefore, the above comparisons clearly demonstrated that the adopted multi-chamber steel tube can aid in enhancing the ultimate carrying capacity of composite columns.

The aspect ratio is another critical parameter that affects the property of M-CFRT stub columns; thus, it was scrutinized. The aspect ratios (B/D) were 2 and 3, and other parameters remained the same as above. Compared with the ultimate bearing capacity of CFST-A1–CFST-A4, that of CFST-A5–CFST-A8 remarkably improved by 33.4%, 37.9%, 39.4%, and 40.8%, respectively, with the aspect ratio increasing from 2 to 3. In summary, the ultimate carrying capacity is considerably affected by the aspect ratio.

3.4. Ductility

In this section, we select the ductility index (DI) [23] as a vital indicator for the compressive performance of M-CFRT stub columns. It is employed to analyze the effect of different factors on the ductility of composite columns. DI is defined as

$$DI = \frac{\varepsilon_{0.85}}{\varepsilon_b} \quad (1)$$

where $\varepsilon_{0.85}$ is the axial strain when the load is reduced to 85% of the ultimate load, ε_b is equal to $\varepsilon_{0.75}/0.75$, and $\varepsilon_{0.75}$ is the axial strain when the load reaches 75% of the ultimate load in the pre-peak stage. $\varepsilon_{0.85}$ and ε_b were derived from Zhang et al. [23]. Figure 8 illustrates a comparison of the DI for all examined columns, calculated using Equation (1). A higher DI indicates a more gradual descent of the curve.

At first, Figure 8 reveals that compared with the DI value of CFST-A1, those of CFST-A2, CFST-A3, and CFST-A4 remarkably improved by 44.1%, 72.9%, and 91.5%, respectively, after welding multiple chambers into the steel tube. Additionally, compared with the DI value of CFST-A5, those of CFST-A6, CFST-A7, and CFST-A8 remarkably improved by 100.4%, 173.9%, and 239.1%, respectively.

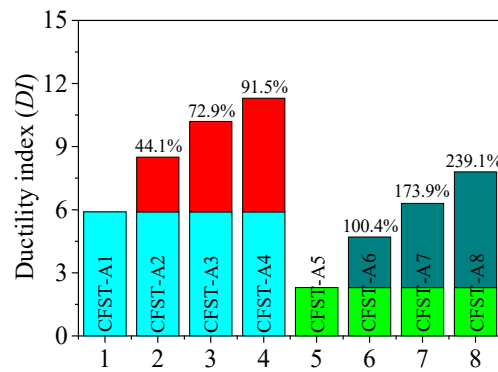


Figure 8. Comparison of ductility index DI for all specimens.

Therefore, the ductility of the composite stub column was improved by the multi-chamber steel tube. In particular, the higher the chamber number in the steel tube is, the better the ductility is. Moreover, in consideration of ductility, the use of M-CFRT stub columns with a multi-chamber steel tube and high-grade concrete is recommended in engineering practices.

4. FEA

4.1. FE Models

Several numerical studies have validated that the compressive performance of CFST columns with various cross-sections can be well and reasonably predicted through refined FE modeling with proper settings.

The FE models were created by ABAQUS/Standard 6.9 software [24], a widely employed tool for investigating the compressive behavior of CFST columns. The C3D8R solid element was used for all components of the composite columns. The mesh size in this study was 10 mm. The loading plate and the model were rigid bodies.

The interfacial behavior between the steel tube and core concrete, where the sliding formulation is finite sliding, was simulated using a surface-based interaction with hard contact in the normal direction and the Coulomb friction coefficient of 0.5 in the tangential direction to the interface. Two distinct surfaces may be coupled by a tie constraint so that no relative motion occurs between them. The interface interaction between different materials was derived from Zhang et al. [23].

The load was imposed by applying a specified displacement. Additionally, all degrees of freedom at the bottom and top ends of the M-CFRT stub columns had constraint. Figure 9 shows the FE models.

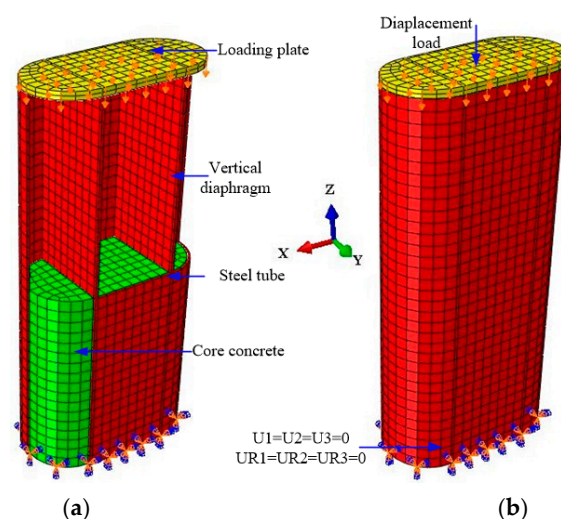


Figure 9. The meshed FE model. (a) Different components element. (b) FE model.

4.2. Material Constitutive Models

In this study, ABAQUS/Standard FE software 6.9 [24] was employed for comprehensive FE modeling. The following stress–strain relationship for concrete under uniaxial compression, presented by Ding et al. [25], was used in the model:

$$y = \begin{cases} \frac{Ax+(B-1)x^2}{1+(A-2)x+Bx^2} & x \leq 1 \\ \frac{x}{\alpha(x-1)^2+x} & x > 1 \end{cases} \quad (2)$$

where the stress and strain ratios of the core concrete to the uniaxial compressive concrete are $y = \sigma/f_c$ and $x = \varepsilon/\varepsilon_c$, respectively. The core concrete's tension and strain are represented by σ and ε . The uniaxial compressive strength of concrete is expressed as $f_c = 0.4f_{cu}^{7/6}$, where f_{cu} is the compressive cubic strength of concrete. The strain associated with the peak compressive stress of concrete is denoted by ε_c , where ε_c is equal to $383f_{cu}^{7/18} \times 10^{-6}$. The parameter A is equal to $9.1f_{cu}^{-4/9}$, which is the ratio of the initial tangent modulus to the secant modulus at peak stress. $B = 1.6(A - 1)^2$ is a parameter that controls the decrease in the elastic modulus along the ascending branch of the axial stress–strain relationship. Parameter α can be assumed to be 0.15 for a steel tubular stub column filled with concrete.

Many experimental studies on the material properties of steel indicate that the constitutive behavior of steel can be described by an elasto-plastic model that takes into account the von Mises yield criteria, the Prandtl–Reuss flow rule, and isotropic strain hardening. This model has been validated in previous studies and is described below:

$$\sigma_i = \begin{cases} E_s \varepsilon_i & \varepsilon_i \leq \varepsilon_y \\ f_y & \varepsilon_y < \varepsilon_i \leq \varepsilon_{st} \\ f_y + \zeta E_s (\varepsilon_i - \varepsilon_{st}) & \varepsilon_{st} < \varepsilon_i \leq \varepsilon_u \\ f_u & \varepsilon_i > \varepsilon_u \end{cases} \quad (3)$$

where σ_i and ε_i are the equivalent stress and strain of the steel. f_y , and $f_u (=1.5 f_y)$ are the yield strength and ultimate strength, respectively. E_s ($=2.06 \times 10^5$ MPa) and E_{st} ($E_{st} = \zeta E_s$) are the elastic modulus and strengthening modulus. ε_y , ε_{st} , and ε_u are the yield strain, hardening strain, and ultimate strain of steel, which are described by $\varepsilon_u = \varepsilon_{st} + 0.5 f_s / (\zeta E_s)$, $\varepsilon_{st} = 12\varepsilon_b$, $\varepsilon_u = 120\varepsilon_b$, and $\zeta = 1/216$.

4.3. Experimental Verification

Based on the above settings, the validation of the FE modeling method involved a comparison between experimental and numerical results, focusing on axial load–strain curves and ultimate bearing capacity. This process assessed the practicality and precision of the modeling approach.

Figure 10 reflects the deformation process of specimens at various stages through axial load–strain curves. Table 1 compares the ultimate bearing capacity values obtained from the experiment ($N_{u,Exp}$) and the corresponding numerical results ($N_{u,FE}$). As shown in Figure 10, almost no differences between measured curves and predicted curves are observed at the initial stage. Moreover, a slight difference is observed between them at other stages, especially for the elastic–plastic stage. This difference exists because although FE models were generated under ideal conditions, preserving the accuracy of measured curves was impossible once concrete crushing and steel tube yielding started. In addition, a reasonable agreement is found, and the average ratio of $N_{u,FE}/N_{u,e}$ is 0.99, with a coefficient of variation of 0.084. Hence, above comparisons show that the FE-simulated curves can show satisfactory and reasonable agreement with the measured curves.

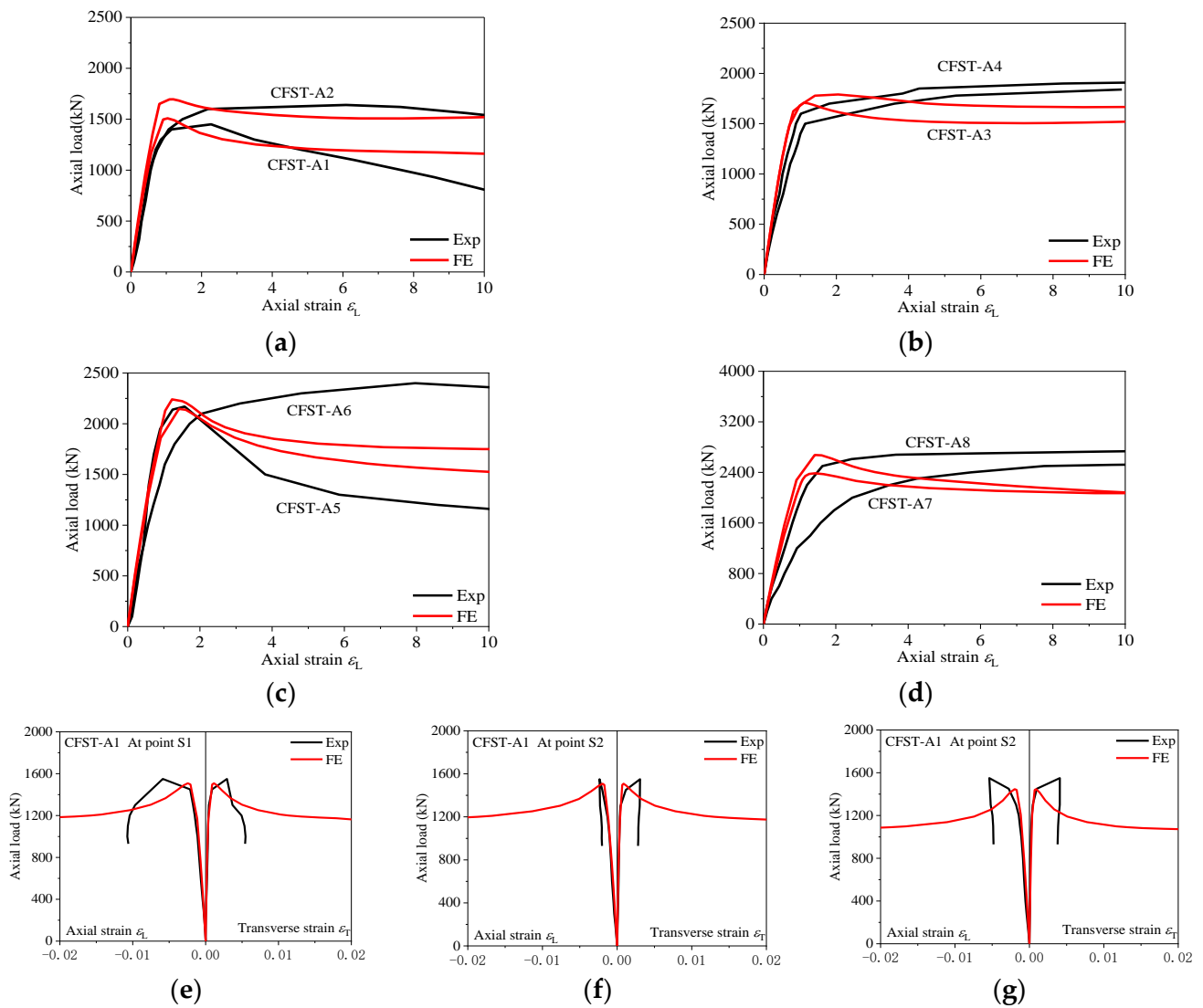


Figure 10. Comparisons of axial load vs. strain curves of specimens between experimental and FE results. (a) CFST-A1 and CFST-A2. (b) CFST-A3 and CFST-A4. (c) CFST-A5 and CFST-A6. (d) CFST-A7 and CFST-A8. (e) CFST-A1 at point S1. (f) CFST-A1 at point S2. (g) CFST-A1 at point S3.

Figure 11 shows the comparison of the stress contour of the core concrete at the ultimate loading state; the blue region represents the unconstrained region of the core concrete. (1) As the chamber in the steel tube is increased, the unconstrained area of the core concrete evidently decreases. (2) Additionally, almost no difference is found in the constrained area of the core concrete on the semicircle cross-section, owing to the strong confinement effect of the circular steel tube on the core concrete. It does not matter how many chambers there are. (3) Most notably, the unconstrained areas of the core concrete between two chambers and four chambers are almost the same, indicating that the steel tube with four chambers cannot remarkably improve the effect of restraint, and the effect of the vertical diaphragm on semicircles on the confinement effect is limited and even neglected.

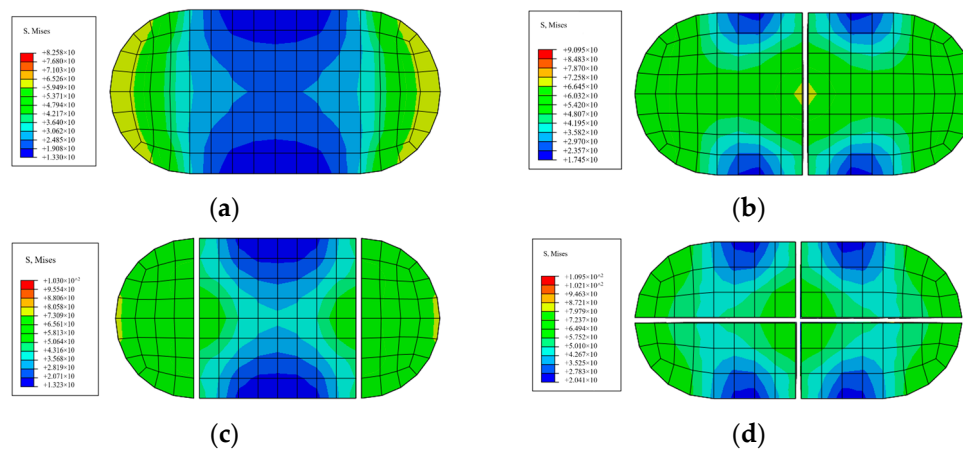


Figure 11. Comparisons of stress contours of the core concrete at the ultimate state. (a) single chambers. (b) two chambers. (c) three chambers. (d) four chambers.

5. Design Approach

Currently, various design formulas are used to determine the ultimate carrying capacity of composite columns, e.g., CFT stub columns with rectangular, square, circular, polygonal, and round-end cross-sections. Nevertheless, M-CFRT stub columns are not covered by the existing design approaches; rather, they are only appropriate for conventional CFT stub columns. In light of the foregoing research, this study aims to provide a novel formula for M-CFRT stub columns.

5.1. Parametric Study

A total of 96 FE models were established in consideration of the following key parameters: concrete strength ranging from C40 to C100, steel strength values of 235, 345, and 420 MPa, aspect ratio ranging from 2 to 4, steel ratio ranging from 0.02 to 0.08, and cell number ranging from 1 to 4. Table 2 lists the detailed parameters of FE models used in the calculation, with the columns with $D = 1200$ taken as examples.

Table 2. Geometric sizes of specimens for parametric study.

D/mm	B/mm	B/D	ρ_s	Cell Number	L/mm
1200	2400	2	0.02~0.08	1~4	5500
	3600	3			5500
	4800	4			7000

Noted: Q235 paired with C40 and C60, Q345 paired with C60 and C80, and Q420 paired with C80 and C100.

5.2. Model Simplification

On the basis of the aforementioned study, the M-CFRT stub columns with three chambers are inferred to have exhibited the optimal compressive performance, followed by the four-, two-, and single-chamber arrangements. In addition, M-CFRT stub columns can be considered a combination of rectangular/square and circular CFT stub columns. Hence, the empirical formula for calculating the ultimate bearing capacity of composite stub columns can be established through the application of the limit equilibrium approach, as outlined in references [3,21].

Numerical results are used to extract the stress distribution at the peak condition of M-CFRT stub columns. The stress envelope of the M-CFRT stub columns can be computed more simply, as illustrated in Figure 12.

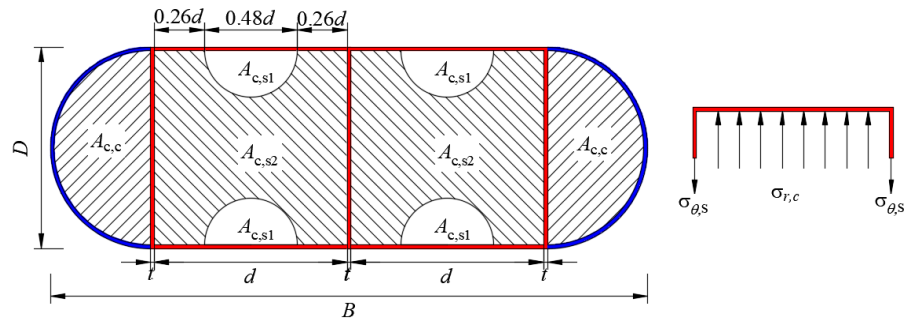


Figure 12. Simplified stress envelope with the mid-section of the M-CFRT stub column.

The reliance on the stress distribution and the unequivocal application of the superposition principle for the concrete cross-section at its peak state are imperative. In this context, A_c represents the overall cross-sectional area of the core concrete, while $A_{c,s2}$ and $A_{c,c}$ denote the areas of the core concrete constrained by square steel tubes and circular steel tubes, respectively. Additionally, $A_{c,s1}$ signifies the unconstrained region of the core concrete. Furthermore, as illustrated in Figure 11, d is the width of the square concrete ($d = D - 2t$). The relationships listed below can be stated in this manner:

$$\begin{cases} A_{c,c} + (n-1)A_{c,s} = A_c \\ A_{c,s1} = 0.18A_{c,s} \\ A_{c,s2} = 0.82A_{c,s} \end{cases} \quad (4)$$

5.3. Formulation

On the basis of the verified FE models, a parametric study on 96 FE full-scale models were further performed to examine the performance of M-CFRT stub columns subjected to axial loading: aspect ratio, which ranges from 1 to 4; steel ration, which ranges from 0.05 to 0.2; concrete strength, which ranges from C40 to C100; and steel yield strength, which ranges from Q235 to Q420.

The longitudinal stress of the square/rectangular steel tube was extracted as soon as the numerical results of the axial load–strain response attained its peak state. Moreover, Figure 13 illustrates the correlation between the ultimate strength ($f_{sc} = N_u / A_{sc}$) and ratio value of axial stress to yield strength for CFT stub columns with square/rectangular cross-sections, where the axial stress of the steel tube is denoted as $\sigma_{L,s}$.

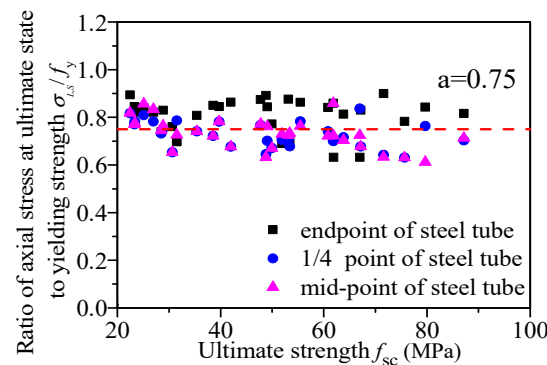


Figure 13. Average ratio of axial compressive stress to yield stress of the steel tube.

As shown in Figure 11, when M-CFRT columns reach their maximum strength, the ratio value of the axial compressive stress to the yield stress is as follows:

$$\sigma_{L,s} = 0.75f_y \quad (5)$$

The tensile transverse stress ($\sigma_{\theta,s}$) of the steel tube can be determined by applying the von Mises yield criterion for steel, as follows:

$$\sigma_{\theta,s} = 0.36f_y \quad (6)$$

As shown in Figure 11, the relationship between the transversal stress ($\sigma_{\theta,s}$) of the steel tube and the radial concrete stress ($\sigma_{r,c}$) of the core concrete at the ultimate state can be expressed as follows:

$$\sigma_{r,c} = \frac{2t\sigma_{\theta,s}}{d} \quad (7)$$

In consideration of the confining stress, the axial compressive stress ($\sigma_{L,c}$) of the core concrete can be expressed as follows:

$$\sigma_{L,c} = f_c + p\sigma_{r,c} \quad (8)$$

where p is the coefficient of lateral pressure ($p = 3.4$) [26].

On the basis of the static equilibrium criterion, the ultimate carrying capacity (N_u) of M-CFRT columns in the mid-height region is categorized into two parts, attributable to the distinct confinement effects of square/rectangular and circular steel tubes on the core concrete: the circular CFT stub column ($N_{u,c}$) and the square/rectangular CFT column ($N_{u,s}$); therefore, this formula can be expressed as

$$N_u = N_{u,c} + N_{u,s} \quad (9)$$

$$N_u = (A_{c,c}f_c + 1.7A_{s,c}f_y) + ((n - 1)\sigma_{L,c}A_{c,s2} + f_cA_{c,s1} + \sigma_{L,s}A_{s,s}) \quad (10)$$

The cross-sectional area of the circular steel tube is denoted as $A_{s,c}$, while the cross-sectional area of the square steel tube is represented as $A_{s,s}$; A_s represents the total cross-sectional area of the steel tube, $A_s = A_{s,c} + A_{s,s}$; and n is the aspect ratio (B/D).

Subsequently, substituting Equations (4)–(8) into Equation (10), the resulting ultimate carrying capacity of the columns (N_u) can be defined as

$$N_u = (A_{c,c}f_c + 1.7A_{s,c}f_y) + ((n - 1)A_{c,s}f_c + 1.25A_{s,s}f_y) \quad (11)$$

$$N_u = A_c f_c + (1.7 A_{s,c} + 1.25 A_{s,s}) f_y \quad (12)$$

Herein, when the aspect ratio ($n = B/D$) is taken as 1, Equation (9) can be expressed as follows:

$$N_u = A_c f_c + 1.7 A_{s,c} f_y \quad (13)$$

The equation denoted by Equation (11), incorporating the confinement effect exerted by a multi-chamber steel tube on the core concrete, is utilized to estimate the ultimate bearing capacity of M-CFRT stub columns. Moreover, it is applicable for predicting the ultimate carrying capacity of circular CFT stub columns, as expressed in Equation (10), namely, M-CFRT stub columns with $B/D = 1$.

5.4. Formula Validation

To confirm the overall applicability and to assess the precision of the proposed formula (Equation (11)), Figure 14 illustrates the comparison of the ultimate carrying capacity between the predicted and FEA results. The comparison involves Eurocode 4 design formulas, comprising 96 FE full-scale models; the ratios represent the values of the predicted outcomes divided by the tested/FE results. The accuracy of the predicted results increases when the average ratio approaches 1.

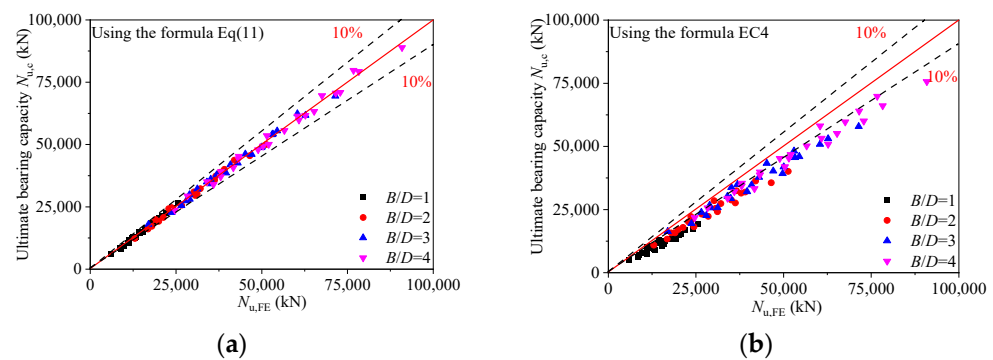


Figure 14. Comparison of the ultimate bearing capacity between FE and predicted results. (a) Formula Equation (11). (b) Eurocode 4.

As depicted in Figure 14a, the average ratio of $N_{u,FE}/N_{u,Eq}$ is 1.00, with a coefficient of variation of 0.032; the absolute average error is 0.026. In this study, the comparisons clearly demonstrate that reasonable agreement is obtained between the numerical results and the corresponding predicted values, suggesting that Equation (11) can be a reasonable estimate for the ultimate carrying capacity.

Meanwhile, Figure 14b shows that the average ratio of $N_{u,FE}/N_{u,EC}$ is 1.20, with a coefficient of variation of 0.080; the absolute average error is 0.143. Evidently, the FE results considerably surpass the corresponding predicted values specified in the standard Eurocode 4 [26], while the predicted strength is relatively conservative. This is because the confinement effects of the semicircle and rectangular steel tube on the core concrete are different in degrees, and both the confinement effects in standard Eurocode 4 are not considered and also overlooked. To sum up, the suggested formula Equation (11) is a reasonable and feasible calculation method.

6. Conclusions

The primary aim of this research is to investigate the compressive behavior of M-CFRT stub columns using a combination of experimental and numerical investigations. The following conclusions can be drawn:

- (1) On the basis of the test results, all the specimens under axial loading are thought to undergo three stages before failing: elastic stage, elastic–plastic stage, and failure stage. Additionally, the vertical diaphragm (chamber number), which can effectively prevent and/or delay the core concrete crushing, essentially changes the failure modes of M-CFRT stub columns. Furthermore, M-CFRT stub columns exhibit greater ductility compared with CFRT stub columns.
- (2) The ultimate carrying capacity and ductility of M-CFRT stub columns remarkably increase with the increase in the chamber number in the steel tube. That is, the axial behavior of M-CFRT stub columns is improved by the multi-chamber steel tube, namely, the vertical diaphragm.
- (3) The observed strong concordance between tested and FE results suggests a favorable agreement. On the basis of these observations, a simplified formula for calculating the ultimate bearing capacity of M-CFRT stub columns is introduced, employing the limit equilibrium method. The predicted results from this formula align well with FE and experimental ones. Consequently, this formula is a reasonable and feasible calculation method for M-CFRT stub columns.

Author Contributions: Software, investigation, data curation, writing—original draft, and funding acquisition, J.L.; methodology, validation, formal analysis, resources, and funding acquisition, T.Z.; conceptualization, writing—review and editing, visualization, supervision, and Funding acquisition, Z.P.; conceptualization, methodology, investigation, resources, and project administration, F.M. All authors have read and agreed to the published version of the manuscript.

Funding: This research is financially supported by the National Natural Science Foundation of China (Nos. 52008159 and 52208220), Hunan Education Department Foundation Funded Project (No. 21A0504), Natural Science Foundation of Hunan Province (No. 2022JJ30112), Aid program for Science and Technology Innovative Research Team in Higher Educational Institutions of Hunan Province, Science and Technology Project of Henan Province (No. 222102320014), Education Reform Research and Practice Project (No. zhjy23-78), Graduate Quality Curriculum Project (No. 2023YJSKC05), Key Research and Development Project of Anhui Province (No. 2022o07020003), Scientific and Technological Project for Housing and Urban–Rural Development in Anhui Province (No. 2023-YF-112), Science and Technology Planning Project of Guichi District, Chizhou City (No. GCKJ202210), and Scientific Research Team Plan of Zhengzhou University of Aeronautics (No. 23ZHTD01009). Their support is gratefully acknowledged.

Data Availability Statement: The data presented in this study are available upon request from the corresponding author. The data are not publicly available due to privacy.

Conflicts of Interest: Authors Zhicheng Pan and Fanjun Ma were employed by the company Sinohydro Engineering Bureau 8 Co., Ltd. Author Zhicheng Pan was employed by the company Power China Chizhou Changzhi Prefabricated Construction Co., Ltd. The remaining authors declare that the research was conducted in the absence of any commercial or financial relationships that could be construed as a potential conflict of interest.

References

1. Shen, Q.H.; Wang, J.H.; Wang, W.Q.; Wang, Z.B. Performance and design of eccentrically-loaded concrete-filled round-ended elliptical hollow section stub columns. *J. Constr. Steel Res.* **2018**, *150*, 99–114. [[CrossRef](#)]
2. Singh, H.; Tiwary, A.K.; Eldin, S.M.; Ilyas, R.A. Behavior of stiffened concrete-filled steel tube columns infilled with nanomaterial-based concrete subjected to axial compression. *J. Mater. Res. Technol.* **2023**, *24*, 9580–9593. [[CrossRef](#)]
3. Ding, F.X.; Fu, L.; Yu, Z.W.; Li, G. Mechanical performances of concrete-filled steel tubular stub columns with round ends under axial loading. *Thin-Walled Struct.* **2015**, *97*, 22–34.
4. Liao, J.; Zeng, J.J.; Quach, W.M.; Zhou, J.K. Axial compressive behavior and model assessment of FRP-confined seawater sea-sand concrete-filled stainless steel tubular stub columns. *Compos. Struct.* **2023**, *311*, 116782. [[CrossRef](#)]
5. Liao, J.; Li, Y.L.; Ouyang, Y.; Zeng, J.J. Axial compression tests on elliptical high strength steel tubes filled with self-compacting concrete of different mix proportions. *J. Build. Eng.* **2021**, *40*, 102678. [[CrossRef](#)]
6. Al-Nini, A.; Nikbakht, E.; Syamsir, A.; Shafiq, N.; Mohammed, B.S.; Al-Fakih, A.; Al-Nini, W.; Amran, Y.M. Flexural behavior of double-skin steel tube beams filled with fiber-reinforced cementitious composite and strengthened with CFRP sheets. *Materials* **2020**, *13*, 3064. [[CrossRef](#)]
7. Xie, J.X.; Lu, Z.A.; Tang, P.; Liu, D. Modal analysis and experimental study on round-ended CFST coupled column cable stayed bridge. In Proceedings of the 2nd International Conference on Mechanic Automation and Control Engineering (MACE), Inner Mongolia, China, 15–17 July 2011; Volume 8, pp. 2302–2304.
8. Xie, J.X.; Lu, Z.A. Numerical simulation and test study on non-uniform areas of round-ended CFST tubular tower. In Proceedings of the Third International Conference on Information and Computing (ICIC2010), Wuxi, China, 4–6 June 2010; Volume 4, pp. 19–22.
9. Al-Fakih, A.; Al-Osta, M.A. Finite element analysis of rubberized concrete interlocking masonry under vertical loading. *Materials* **2022**, *15*, 2858. [[CrossRef](#)] [[PubMed](#)]
10. Gong, F.; Maekawa, K. Multi-scale simulation of freeze-thaw damage to RC column and its restoring force characteristics. *Eng. Struct.* **2018**, *156*, 522–536. [[CrossRef](#)]
11. Zhu, X.; Abe, H.; Hayashi, D.; Tanaka, H. Behavioral characteristics of RC beams with non-uniform corrosion along the reinforcement. *J. Intell. Constr.* **2023**, *1*, 9180019. [[CrossRef](#)]
12. Li, P.; Wang, H.; Nie, D.; Wang, D.; Wang, C. A method to analyze the long-term durability performance of underground reinforced concrete culvert structures under coupled mechanical and environmental loads. *J. Intell. Constr.* **2023**, *1*, 9180011. [[CrossRef](#)]
13. Wan, C.Y.; Zha, X.X. Nonlinear analysis and design of concrete-filled dual steel tubular columns under axial loading. *Steel Compos. Struct.* **2016**, *20*, 571–597. [[CrossRef](#)]
14. Zhu, A.Z.; Zhang, X.W.; Zhu, H.P.; Zhu, J.H.; Lu, Y. Experimental study of concrete filled cold-formed steel tubular stub columns. *J. Constr. Steel Res.* **2017**, *134*, 17–27. [[CrossRef](#)]
15. Wang, J.F.; Shen, Q.H.; Jiang, H.; Pan, X.B. Analysis and design of elliptical concrete filled thin-walled steel stub columns under axial compression. *Int. J. Steel Struct.* **2018**, *18*, 365–380. [[CrossRef](#)]
16. Zhao, Y.G.; Yan, X.F.; Lin, S.Q. Compressive strength of axially loaded circular hollow centrifugal concrete-filled steel tubular short columns. *Eng. Struct.* **2019**, *201*, 109828. [[CrossRef](#)]
17. Pi, T.; Chen, Y.; He, K.; Han, S.H.; Wan, J. Study on circular CFST stub columns with double inner square steel tubes. *Thin-Walled Struct.* **2019**, *140*, 195–208. [[CrossRef](#)]

18. Zhou, F.; Young, B. Experimental investigation of concrete-filled single-skin and double-skin steel oval hollow section stub columns. *Thin-Walled Struct.* **2019**, *140*, 157–167. [[CrossRef](#)]
19. Han, L.H.; Ren, Q.X.; Li, W. Tests on stub stainless steel-concrete-carbon steel double-skin tubular (DST) columns. *J. Constr. Steel Res.* **2011**, *67*, 437–452. [[CrossRef](#)]
20. Wang, J.F.; Shen, Q.H. Numerical analysis and design of thin-walled RECFST stub columns under axial compression. *Thin-Walled Struct.* **2018**, *129*, 166–182. [[CrossRef](#)]
21. Ding, F.X.; Fu, L.; Liu, X.M.; Liu, J. Mechanical performances of track-shaped rebar stiffened concrete-filled steel tubular (SCFRT) stub columns under axial compression. *Thin-Walled Struct.* **2016**, *99*, 168–181. [[CrossRef](#)]
22. GB 50017-2003; Code for Design of Steel Structures. China Planning Press: Beijing, China, 2003.
23. Zhang, T.; Ding, F.X.; Wang, L.P.; Liu, X.M.; Jiang, G.S. Behavior of polygonal concrete-filled steel tubular stub columns under axial loading. *Steel Compos. Struct.* **2018**, *28*, 573–588.
24. Smith, M. *ABAQUS/Standard User's Manual, Version 6.9*; Dassault Systèmes Simulia Corp.: Providence, RI, USA, 2009.
25. Ding, F.X.; Ying, X.Y.; Zhou, L.C.; Yu, Z.W. Unified calculation method and its application in determining the uniaxial mechanical properties of concrete. *Front Struct. Civ. Eng.* **2011**, *5*, 381–393. [[CrossRef](#)]
26. EN 1994-1-1:2004; Design of Composite Steel and Concrete Structures Part1-1: General Rules-Structural Rules for Buildings. European Committee for Standardization: Brussels, Belgium, 2004.

Disclaimer/Publisher's Note: The statements, opinions and data contained in all publications are solely those of the individual author(s) and contributor(s) and not of MDPI and/or the editor(s). MDPI and/or the editor(s) disclaim responsibility for any injury to people or property resulting from any ideas, methods, instructions or products referred to in the content.